## SUPPLEMENTARY INFORMATION

Hyperpixels: Pixel Filter Arrays of Multivariate Optical Elements for Optimized Spectral Imaging

Calum Williams<sup>1</sup>, Richard Cousins<sup>2</sup>, Christopher J. Mellor<sup>3</sup>, Sarah E. Bohndiek<sup>45</sup>, and George S. D. Gordon<sup>6\*</sup>

<sup>1</sup>Department of Physics, University of Exeter, Exeter, EX4 4QL, United Kingdom

<sup>2</sup>Nano- and Micro-scale Research Centre, University of Nottingham, University Park, Nottingham, NG7 2RD, UK

<sup>3</sup>School of Physics and Astronomy, University of Nottingham, University Park, Nottingham, NG7 2RD, UK

<sup>4</sup>Department of Physics, Cavendish Laboratory, University of Cambridge, JJ Thomson Avenue, Cambridge, CB3 0HE, UK

<sup>5</sup>Cancer Research UK Cambridge Institute, University of Cambridge, Robinson Way, Cambridge, CB2 0RE, UK

Optics & Photonics Research Group, Department of Electrical and Electronic Engineering, University of Nottingham, Nottingham, NG7 2RD, UK

\*Correspondence: George Gordon (george.gordon@nottingham.ac.uk)

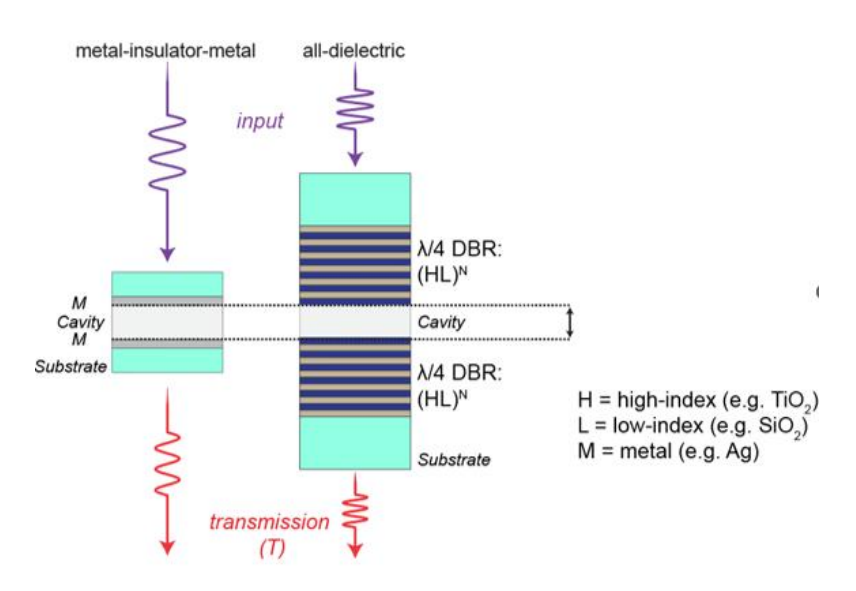


**Figure S1.** Simple Fabry-Perot filter: metal-insulator-metal vs. all-dielectric structure. DBR = distributed Bragg reflector (i.e. dielectric broadband mirror). N = number of bi-layers

A conventional Fabry-Perot narrowband filter (etalon) is composed two parallel mirrors separated by a finite thickness cavity (spacer layer, usually an insulator). Light incident upon the structure undergoes partial reflection and transmission through the mirrors. Constructive interference conditions within the resonant cavity give rise to a series of sharp transmission peaks and through control of parameters such as cavity optical thickness and material selection, the wavelengths of the transmissive light can be tuned [1,2]. Two common Fabry-Perot filter designs exist: (i) metal-insulator-metal (MIM), and (ii) all-dielectric (**Figure 1**). For a planar MIM case, the generalized constructive interference condition (at normal incidence) is give as,

$$2 \operatorname{Re}[\tilde{n}]d = m\lambda + \phi$$
  $m = 1,2,\cdots$ 

where  $\tilde{n}$  is the complex refractive index of the cavity (insulator), where the Re part determines phase velocity and the Im part determines loss, d is the cavity physical thickness, m is an integer,  $\lambda$  is the wavelength of light, and  $\phi$  is the phase shift due to effect of reflection of the mirror materials. Note that this phase shift is significant for metallic mirrors compared to all-dielectric interferaces. Due to the presence multiple dispersive and lossy materials in a realistic MIM system (i.e. noble metals, adhesion layers etc.) it's often necessary to implement numerical modelling approaches. For 1D thin-film multilayer designs, the transfer matrix method (TMM) is traditionally implemented, also used in this work (through TFCalc and Lumerical STACK simulations). To determine the reflectance of a lossy periodic structure, recursive propagation matrices are used [1-3]. For M thin-film slabs, M+1 interfaces, with reflection coefficients,  $\rho_i$ , at each interface (assuming normal incidence) is given by,

$$\rho_i = \frac{\left[\tilde{n}(\omega)\right]_{i-1} - \left[\tilde{n}(\omega)\right]_i}{\left[\tilde{n}(\omega)\right]_{i-1} + \left[\tilde{n}(\omega)\right]_i} \qquad i = 1, 2, \dots M + 1$$

where  $\tilde{n}(\omega)_i$  is the complex refractive associated with the i-th slab. The *propagation transfer matrix*, to describe the forward and backward electric field propagation within the multilayer stack [2], is given by

$$\begin{bmatrix} E_{i+} \\ E_{i-} \end{bmatrix} = \frac{1}{\tau_i} \begin{bmatrix} 1 & \rho_i \\ \rho_i & 1 \end{bmatrix} \begin{bmatrix} e^{j\delta_i} & 0 \\ 0 & e^{-j\delta_i} \end{bmatrix} \begin{bmatrix} E_{i+1,+} \\ E_{i-1,-} \end{bmatrix} \qquad i = M, M-1, \cdots 1$$

where  $\delta_i=k_{zi}l_i$ , is the complex phase thickness,  $k_{zi}=k_0\big[\tilde{n}_{eff}\big]_i$ , where  $k_0=2\pi/\lambda_0$ , is the free-space wavenumber and  $\tau_i=1+\rho_i$  is the transmission coefficient. Hence, every recursion calculation is computed for every wavelength. The *reflection response*, considering the wavelength-dependent fields at each interface, given generally by  $\Gamma_i=E_{i+}/E_{i-}$ , is described by [1,2]:

$$\Gamma_i = \frac{\rho_i + \Gamma_{i+1} e^{-2j\delta_i}}{1 + \rho_i \Gamma_{i+1} e^{-2j\delta_i}}$$
  $i = M, M - 1, \dots 1$ 

With the *transmission response* counterpart given,

$$T_i = \frac{\tau_i T_{i+1}}{1 + \rho_i \Gamma_{i+1} e^{-2j\delta_i}}$$
  $i = M, M - 1, \dots 1$ 

The multiplicative interaction of these responses give rise to the total transmission from the stack – which generally is composed of,

$$egin{pmatrix} n_1 \\ n_2 \\ n_3 \\ n_4 \\ n_5 \\ n_6 \\ n_7 \\ n_8 \\ n_9 \end{pmatrix} = egin{pmatrix} n_{air} = 1 \\ n_{capping} \\ ilde{n}_{M} \\ ilde{n}_{adhesion} \\ ilde{n}_{M} \\ ilde{n}_{capping} \\ ilde{n}_{adhesion} \\ ilde{n}_{alass} = 1.52 \end{pmatrix}$$

The physical thickness of each layer is iterated in the simulations, along with material selection for the capping and adhesion layers.  $\tilde{n}_M$ = the complex index of Ag mirror, and  $\tilde{n}_I$ = the complex index of the photoresist (ARN-7720, AllResist) insulator. Due to the dispersive and lossy behaviour of Ag and Ti (adhesion), the filtering performance is sub-optimal. That is, in comparison to negligible loss dielectric counterpart structures which exhibit near unity transmission peaks with narrowband filtering, the MIM structures exhibit broader passbands, reduced transmission peaks and non-broadband performance i.e. the nature of interband transition in the UV-blue part of the waveband mean transmission peaks are not equal in max value, with background signal is inversely proportional to wavelength. **Figure 2** overviews the total transmission response of conventional all-dielectric thin-film bandpass filters as thin film structure changes. **Figures 3, 4** and **5** overview a comparative MIM bandpass filter structure, and show the non-idealised performance.

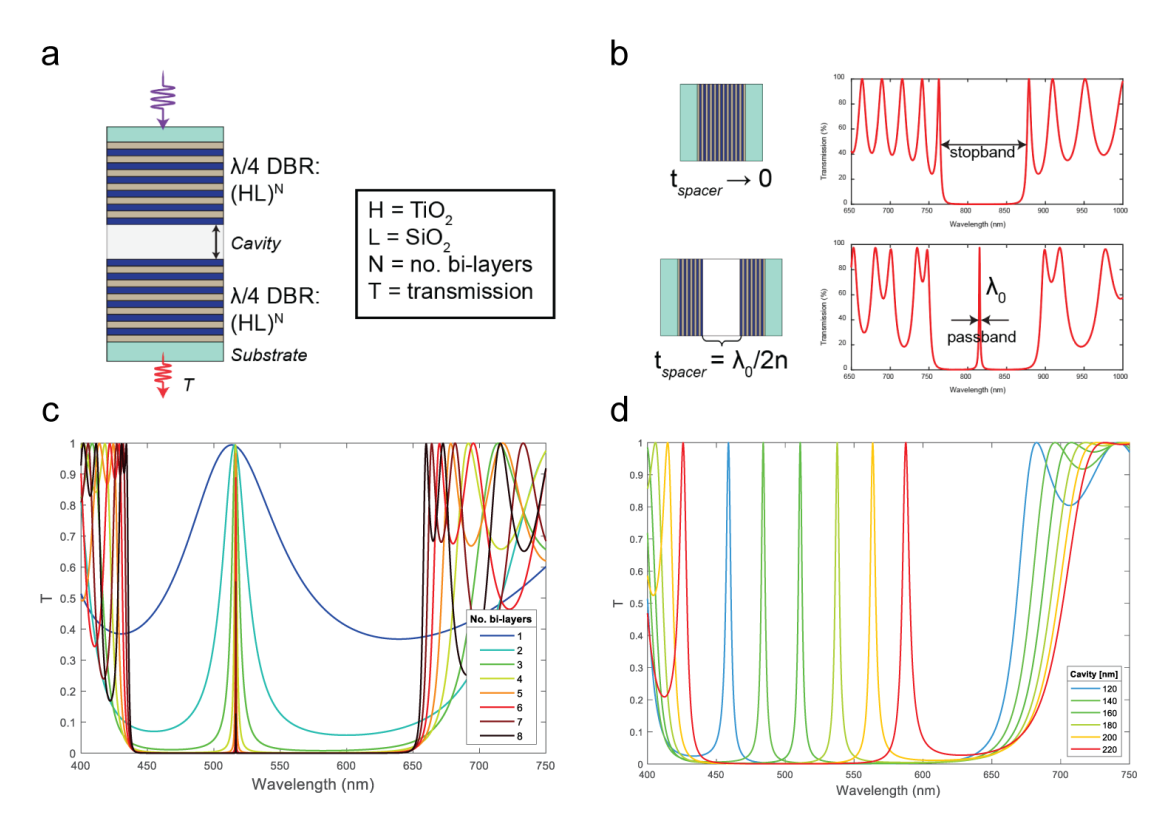


**Figure S2.** (a) Structure of a conventional thin-film all-dielectric Fabry-Perot bandpass filter. (b) Simulation of the transmission response of two geometries: top – a Bragg mirror only, which exhibits a broad stopband with a function of the difference in index between H-L layer materials; bottom – by introducing a cavity (defect) between two Bragg mirrors a passband arises, with a constructive interference condition. This leads to the widespread optical bandpass filter. (c) The effect of increasing the number of H-L bi-layers on the transmission response results in a narrower passband and lower out of band rejection. (d) Increasing the cavity thickness red-shifts the centre wavelength of the passband, explained by the change in the constructive interference condition. Note: these resonances are of 1st order here, and the 2<sup>nd</sup> order of the thickest cavity can be observed in the blue part of the spectrum.

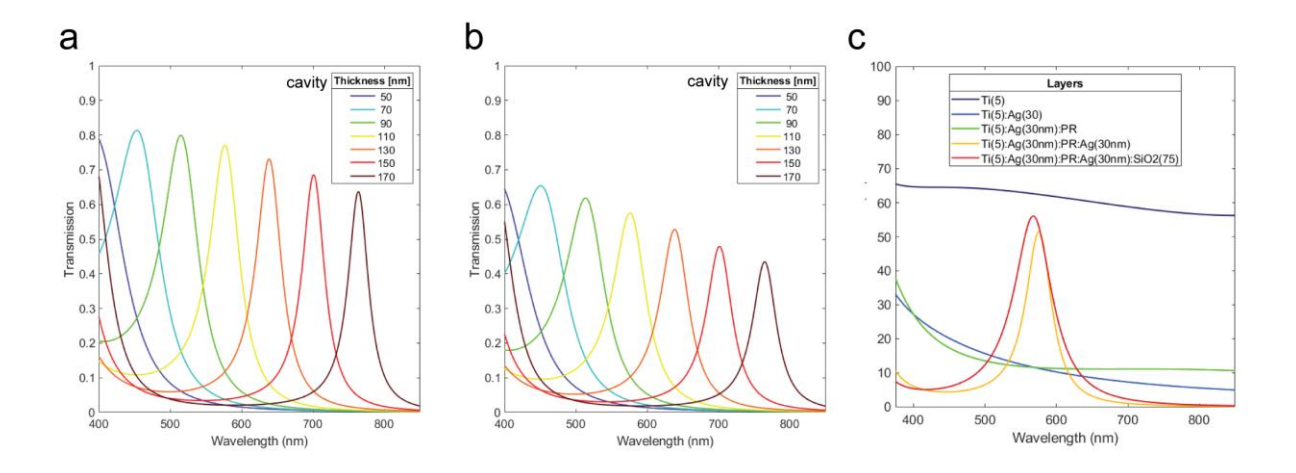


**Figure S3.** Simulated total transmission response of multi-layer MIM structures using TFCalc. (a) Transmission response of idealized structure with varying cavity thickness variation, structure: Glass (bulk): Ag (mirror)[30 nm]: MgF<sub>2</sub> (capping)[15 nm]: photoresist (cavity)[~]: Ag mirror[30 nm]: MgF<sub>2</sub> (capping)[50 nm]: air. (b) Same as (a), but with structural addition of 1 nm Ti adhesion layer underneath each mirror layer, which introduces loss thereby broadening the passbands and lowering the peak transmission. (c) Total transmission response of building the MIM multi-layer structure (one layer at a time) to show the effect of adding each layer.

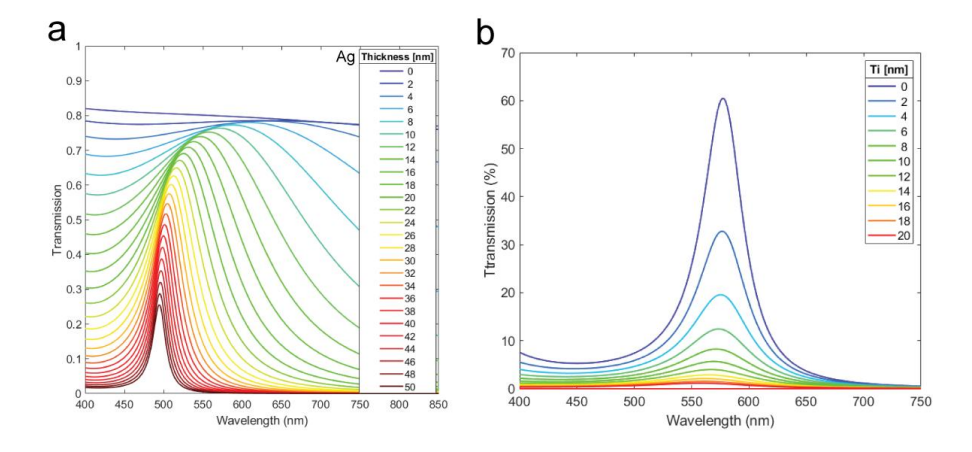


**Figure S4.** (a) Simulated total transmission response of MIM structure—as in Figure 2(b)—with increasing Ag thickness, which demonstrates the effects of: introducing a necessary mirror reflective phase shift to generate a constructive inference condition thereby giving rise to a bandpass, but also with increasing thickness introducing more loss resulting in a lower transmission peak, this tradeoff is considering part of the design process for the final MSFA filter thicknesses and end imaging requirements (i.e. optical throughput vs. narrowness of response). (b) Effect of increasing the Ti adhesion layer thickness on a MIM structure's transmission (with fixed mirror and cavity thicknesses). The increase in Ti thickness dampens the resonance due to additional loss, thereby significantly cutting the transmitted signal. Tradeoff for practical MSFA due to needing the mirrors to adhere to the substrates while maintaining a sufficiently strong signal.

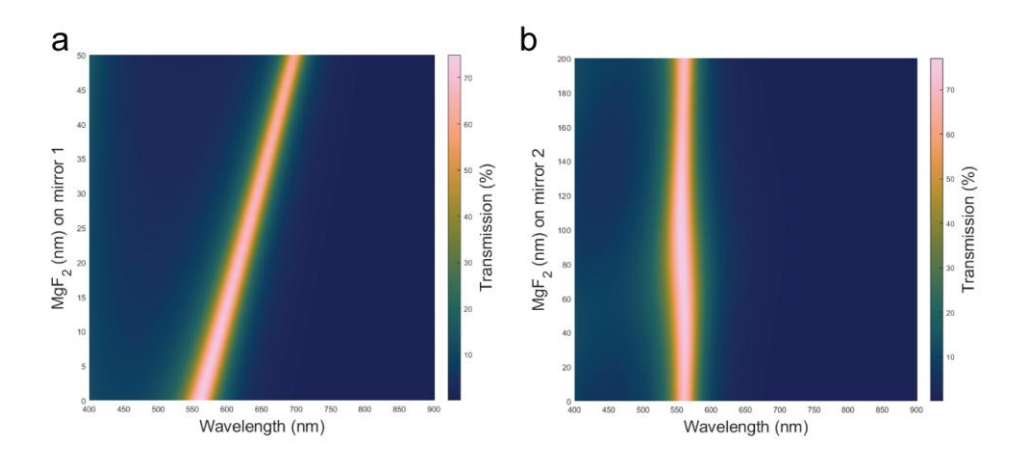


**Figure S5.** Effect on total transmission response of a MIM structure with variable thickness  $MgF_2$  capping (encapsulation) layer atop Ag mirror 1 (a) and Ag mirror 2 (b). Increasing the capping thickness on mirror 1 (facing the cavity) introduces an additional optical thickness thereby red-shifting the wavelength. Whereas on mirror 2, negligible spectral shift, but there is an optimal thickness based on impedance matching with air. Note that additional practical consideration is also minimum thicknesses of a capping layer of Ag in order to prevent tarnishing / oxidation over longer periods of time.

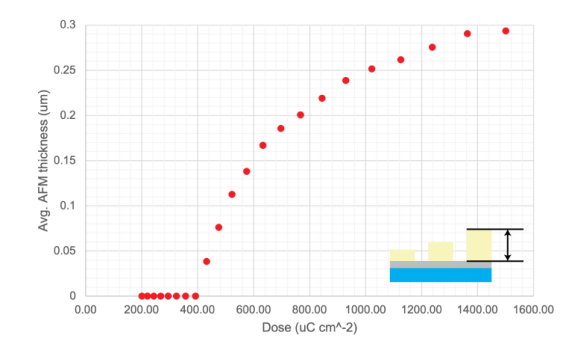


**Figure S6.** Experimental dose test thickness results of undiluted ARN-7720.13 e-beam resist (without paper specific dilution) [spin speed 5,000 rpm; bake 85degC, 2min; 1 min development] obtained through AFM measurements of isolated chequerboard arrays.

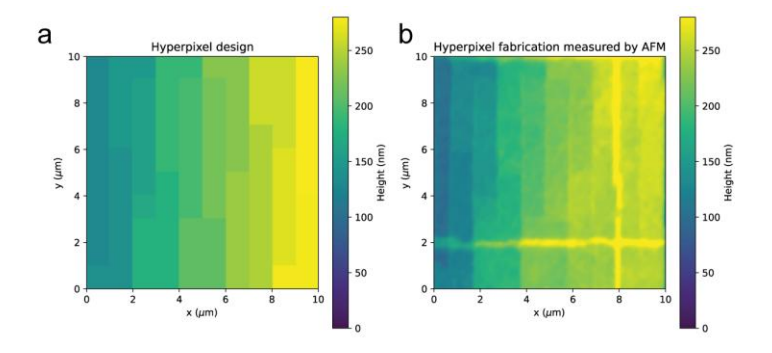


**Figure S7.** Comparison of thickness map of (a) hyperpixel design, vs. (b) fabricated hyperpixel (AFM micrograph). There is sub-pixel variation (for example due to the nature of the resist dissolution process) which gives rise to broadened passbands, however there is general agreement between maps.

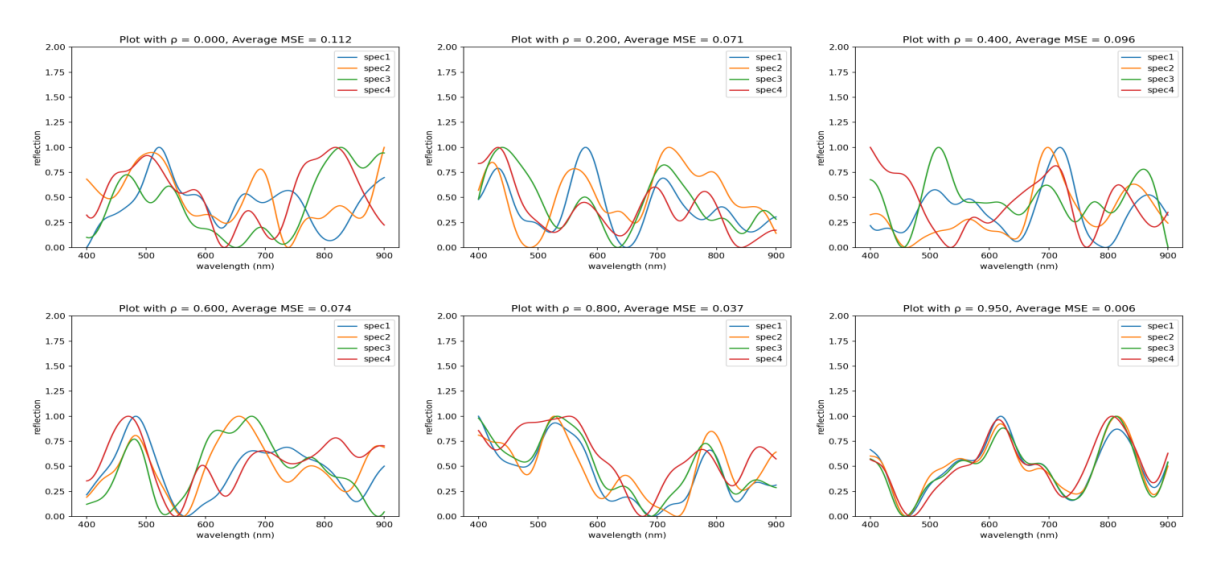


**Figure S8.** Illustration of how varying the  $\rho$  parameter in our simulation generates realistic, randomized spectra with controllable degrees of correlation. The average mean-squared error (MSE) between each pair of spectra is shown, decreasing from 0.112 at  $\rho$  = 0.00 to 0.006 at  $\rho$  = 0.95.

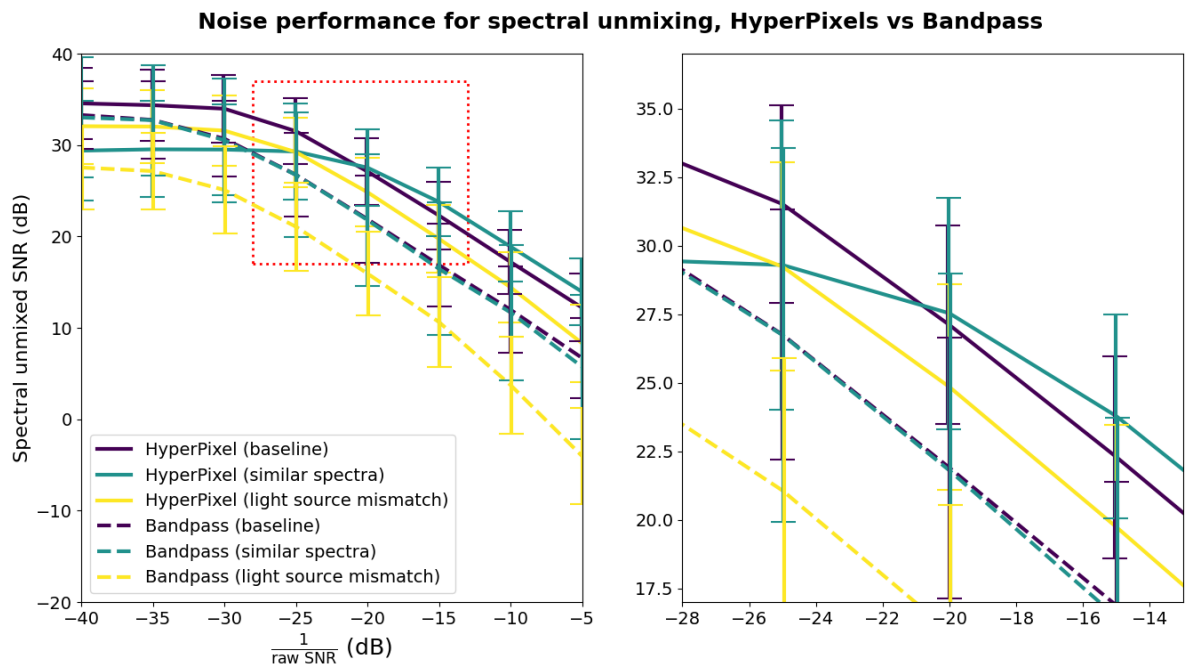


**Figure S9.** Simulation results demonstrating the signal-to-noise ratio (SNR) advantage of hyperpixel designs over optimized bandpass filter designs in edge cases. The simulations consider a scenario where spectra are highly similar ( $\rho$  = 0.95, average mean-squared error = 0.006) compared to the baseline case ( $\rho$  = 0.00, average mean-squared error = 0.112). See Supplementary Figure 8 for example spectra. When data noise levels approaches zero (SNR gets large), conventional bandpass filters provide an SNR unmixing advantage of 3.7 dB compared to hyperpixels. However, as data noise increases to realistic levels (SNR < 20 dB) , the SNR advantage of hyperpixels grows to 7 dB over bandpass filters, highlighting their robustness under adverse conditions. The simulations also examine the case of mismatched illumination, in which hyperpixels and bandpass filters are optimized for a flat-spectrum light source but are tested with a broadband, non-flat halogen source (ThorLabs OSL2). Under low data noise, hyperpixels provide a 4.5 dB SNR unmixing advantage over optimized bandpass filters, increasing to over 9 dB, further demonstrating the robust of hyperpixels in these edge cases.

## Graph showing effect of spectral normalization

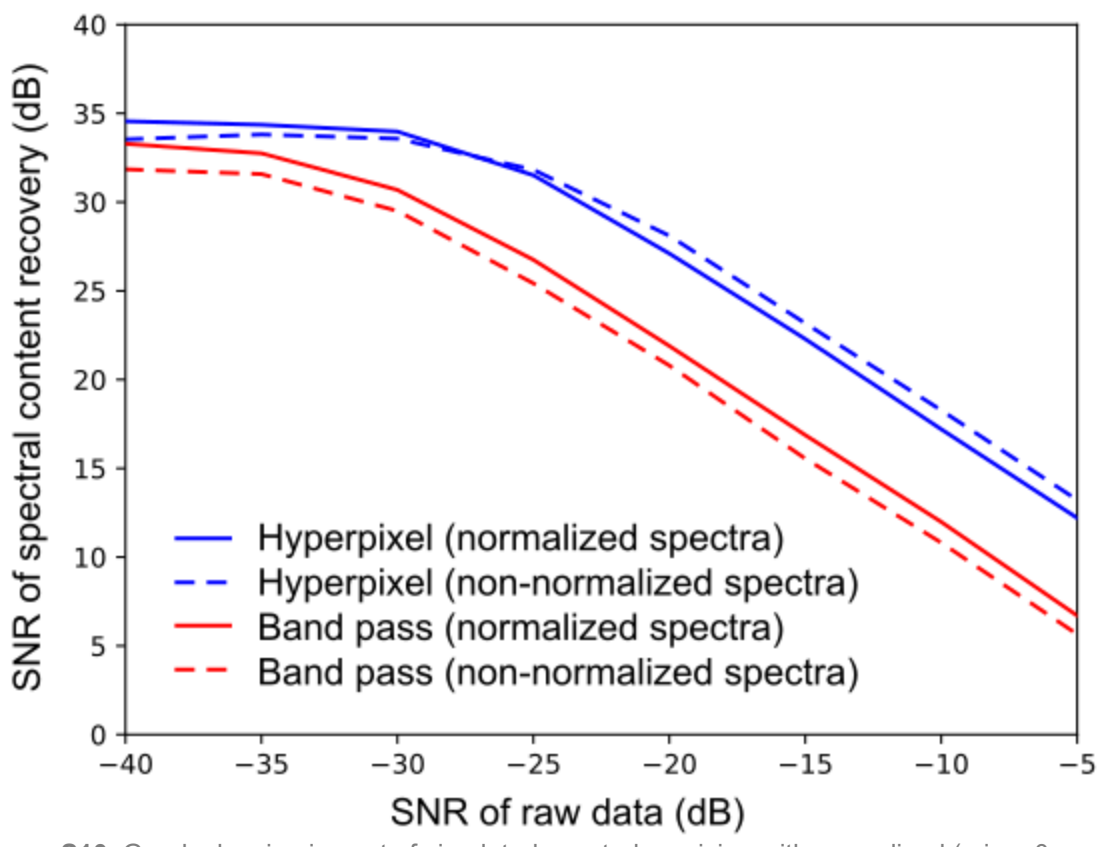


**Figure S10.** Graph showing impact of simulated spectral unmixing with normalized (min = 0, max = 1) and non-normalized (max and min both in range [0,1]) spectra. Normalized spectra actually represent a more challenging practical case, with the gap between band pass and hyperpixels growing by >2 dB. In both cases, however, there is still a clear performance advantage of hyperpixels over conventional bandpass filters.

## References

- [1] Macleod, H. Thin-Film Optical Filters, third ed.; Institute of Physics Publishing, 1986.
- [2] Orfanidis, S.J. Electromagnetic Waves and Antennas, vol. 2, electronic ed., 2008
- [3] Kajtár, G., Kafesaki, M., Economou, E. N. & Soukoulis, C. M. Theoretical model of homogeneous metal-insulator-metal perfect multi-band absorbers for the visible spectrum. J. Phys. D. Appl. Phys. 49, 55104 (2016).